

ANL-HEP-PR-98-46  
May, 1998

# Long-Range Correlations in Deep-Inelastic Scattering

S.V.Chekanov <sup>1</sup>

Argonne National Laboratory, 9700 S.Cass Avenue,  
Argonne, IL 60439 USA

Short title: Long-Range Correlations in DIS

## Abstract

Multiplicity correlations between the current and target regions of the Breit frame in deep-inelastic scattering processes are studied. It is shown that the correlations allow one to tag the first-order perturbative QCD effects and can be used to extract the behavior of the boson-gluon fusion rates as a function of the Bjorken variable. The behavior of the correlations is derived analytically and analyzed using a Monte Carlo simulation.

---

<sup>1</sup>On leave from Institute of Physics, AS of Belarus, Skaryna av.70, Minsk 220072, Belarus.

# 1 Introduction

Long-range correlations in rapidity have been studied for many years in  $e^+e^-$ ,  $\mu^+p$ ,  $\nu p$ ,  $\bar{\nu}p$ ,  $pp$ ,  $p\bar{p}$ ,  $\pi^\pm p$ ,  $K^+p$ , and  $e^+p$  collisions in forward-backward event hemispheres. Results for  $e^+e^-$ ,  $\mu^+p$  processes indicated that such correlations are small at energies studied in [1, 2]. At LEP1 energies, DELPHI, OPAL and ALEPH collaborations observed positive long-range correlations, mainly due to heavy quark pair production [3–5]. For  $\nu p$  and  $\bar{\nu}p$  processes, the correlations are rather small and negative [6]. For  $pp$ ,  $p\bar{p}$  [7] and  $\pi^\pm p$ ,  $K^+p$  [8] collisions, the correlations are large positive and increase with  $\sqrt{s}$ . Recently, it was shown that the long-range correlations defined in the  $\gamma^*\mathbb{P}$  center-of-mass system of diffractive  $e^+p$  collisions are positive [9].

In this paper we discuss the measurements of the long-range correlations in neutral current deep-inelastic scattering  $e^+p$  collisions using the Breit frame [10]. We estimate analytically the correlations from the first-order QCD (Sect. 3) and compare them with a Monte Carlo simulation (Sect. 4).

## 2 Definitions

The event kinematic of the deep-inelastic processes is determined by the 4-momentum transfer  $Q^2 = -q^2$ , and the Bjorken scaling variable  $x = Q^2/(2Pq)$ , where  $P$  is the 4-momentum of the proton. To study the correlations, we use the Breit frame. In the quark-parton model (QPM), the Breit frame provides the maximum separation between the radiation from the outgoing struck quark and that from the proton remnant. In this frame the incident quark carries momentum  $Q/2$  in the positive  $z$ -direction and the outgoing struck quark carries  $Q/2$  in the negative  $z$ -direction. The phase space of the event can be divided into two regions. All particles with negative  $p_z$  components of momenta form the current region, which is analogous to a single hemisphere of  $e^+e^-$  collisions. In the QPM, all these particles are produced due to the hadronization of the struck quark. Particles with positive  $p_z$  are assigned to the target region, which is associated with the proton remnant (see Fig. 1).

Long-range correlations deal with the problem of a possible interdependence of different, well-separated phase-space regions of multiparticle production. For the Breit frame, it is natural to ask whether the current and target regions are independent of each other. Assuming that a color flow between the struck quark and the proton remnant at the fragmentation stage cannot produce strong correlations, one may think that the radiation of the struck quark should be independent of the target region. Below we shall show that, generally, such an expectation is not correct when QCD corrections to the QPM are considered.

To study a possible correlation between the current and target region, we use the covariance:

$$\rho \equiv \text{cov}(n_c, n_t) = \langle n_c n_t \rangle - \langle n_c \rangle \langle n_t \rangle, \quad (1)$$

where  $n_c$  ( $n_t$ ) is the number of particles in the current (target) region,  $\langle \dots \rangle$  is average over all events.

There are a few well established statistical properties of the  $\rho$ :

1. Fully independent particle production in the current and target regions implies  $\rho = 0$ .
2. Since  $\rho$  represents a degree of linear stochastic dependence between  $n_c$  and  $n_t$ , more complex forms of interdependence are not described by this variable. Therefore, the fact that  $\rho = 0$  is still not evidence for absence of correlations.
3. Positive correlation leads to  $\rho > 0$ , negative one produces  $\rho < 0$ .

The forward-backward correlations have been studied earlier in terms of the parameter  $b$  which is given by the slope in the linear relation  $\langle n_F \rangle = a + b n_B$ , where  $n_F$  ( $n_B$ ) is the number of particles in forward (backward) hemispheres. The parameter  $b$  is directly related to the covariance  $\rho$  and can be defined [11] using the standard deviation  $\sigma_F$  for the forward hemisphere,

$$b = \sigma_F^{-2} \rho. \quad (2)$$

For the present study we shall use the  $\rho$  rather than  $b$ . While the statistical content of the both quantities is same, the covariance is easier to obtain both analytically and experimentally.

Having established all these notations and definitions, below we shall analytically estimate the covariance  $\rho$  using first-order QCD effects.

### 3 QCD expectation

Going from the quark-parton model to the first-order QCD description means to consider more complex processes. In Born approximation, Boson-Gluon Fusion (BGF) and QCD-Compton scattering (QCDC) can significantly contribute to the overall topology of the events (see Fig. 2). Both processes lead to (2+1) partons, where “1” denotes the proton remnant. While in the QPM the quark has  $p_z = Q/2$  before and  $p_z = -Q/2$  after the collision, the first-order QCD processes make the collision in the Breit frame no longer collinear, although the target and current regions are still well defined operationally.

Following [12], different event configurations of (2+1) jets in the Breit frame are shown in Fig. 3. The configurations are defined according to the longitudinal momenta of jets induced by the first-order QCD processes. For the first configuration both jets from the first-order QCD processes are moving backward to the current

region. For the next two topologies (see b) and c)), the two jets are produced back-to-back with one jet in the current and one in the target region. (Both jets may have different longitudinal momentum, but this does not affect the QCD estimate of correlations to be made below.) For the topology d), the two jets are produced in the target region. Note that, for the Breit frame, the latter topology is not in conflict with longitudinal momentum conservation [12].

Let now estimate the covariance  $\rho$  analytically. If  $h$  particles migrate to the target region, one can rewrite (1) as

$$\rho = \langle (\tilde{n}_c - h) (\tilde{n}_t + h) \rangle - \langle \tilde{n}_c - h \rangle \langle \tilde{n}_t + h \rangle. \quad (3)$$

Here  $\tilde{n}_c$  is the number of particles emitted due to zero and first-order QCD processes and  $\tilde{n}_t$  is the multiplicity of the proton remnant without counting the particles migrating from the first-order QCD processes. From (3) one obtains

$$\rho = \langle \tilde{n}_c h \rangle - \langle \tilde{n}_c \rangle \langle h \rangle - \langle h^2 \rangle + \langle h \rangle^2. \quad (4)$$

In this expression, the contributions from the remnant multiplicity  $\tilde{n}_t$  cancel since we consider the case when  $\tilde{n}_t$  is independent of  $\tilde{n}_c$  and  $h$ . This assumption means that the only dominant effect leading to the correlation between  $n_c$  and  $n_t$  is the first-order QCD migration shown in Fig. 3, rather than non-perturbative effects. The validity of this assumption will be tested using a Monte Carlo simulation in Sect. 4.

We do not consider the configuration a) anymore since it cannot contribute to the correlation ( $h = 0$ ). This configuration is rather similar to the QPM events but only with large transverse momenta of both jets. Because of this, it is possible that some particles migrate to the target region due to the parton showering or resonance decays. However, these effects are expected to be small.

Now let us define the production rate  $R_b$  for the back-to-back jets (see b) and c) in Fig. 3) and the production rate  $R_f$  for the events with both jets moving forward to the target region (see d)) as

$$R_b = \frac{N_b}{N_{\text{ev}}}, \quad R_f = \frac{N_f}{N_{\text{ev}}}, \quad (5)$$

where  $N_b$  is the number of back-to-back jet events,  $N_f$  is the number of events without activity in the current region and  $N_{\text{ev}}$  is the total number of events. We consider these definitions in the limit  $N_{\text{ev}} \rightarrow \infty$ , so that  $R_b$  and  $R_f$  are the probabilities of having each configuration.

For every first-order QCD event with a total multiplicity  $w$ , the number  $h$  of particles moving to the target region is about  $w/2$  for the back-to-back jets, and  $w$  for events without particles in the current region. Using this estimate, one can write the following set of relations:

$$\langle \tilde{n}_c h \rangle \simeq \langle w^2 \rangle [0.5R_b + R_f], \quad (6)$$

$$\langle \tilde{n}_c \rangle \langle h \rangle \simeq \langle w \rangle \langle \tilde{n}_c \rangle [0.5R_b + R_f], \quad (7)$$

$$\langle h^2 \rangle \simeq \langle w^2 \rangle [0.25R_b + R_f], \quad (8)$$

$$\langle h \rangle^2 \simeq \langle w \rangle^2 [0.5R_b + R_f]^2. \quad (9)$$

Note that the averaging for  $w$  is performed only over the relevant first-order QCD events. The term (9) can safely be ignored since  $R_b, R_f \ll 1$ ,  $\langle w \rangle^2 < \langle w^2 \rangle$ . Combining (6)-(8) together, one obtains from (4)

$$\rho \simeq -\langle w \rangle \langle \tilde{n}_c \rangle [0.5R_b + R_f] + 0.25 R_b \langle w^2 \rangle. \quad (10)$$

The similarity with  $e^+e^-$  annihilations makes it possible to estimate  $\langle w^2 \rangle$ . The distribution of the multiplicity  $w$  in the two-jet events of the  $e^+e^-$  collisions is usually well fitted by a negative-binomial distribution for which the following relation holds.

$$\langle w^2 \rangle = \langle w \rangle^2 (1 + k^{-1}) + \langle w \rangle, \quad (11)$$

with a free parameter  $k$  which is much larger than one ( $k = \infty$  for a Poisson distribution). Using this relation, one obtains

$$\rho \simeq -A_b R_b - A_f R_f, \quad (12)$$

$$A_b = \langle w \rangle \langle \tilde{n}_c \rangle \left[ \frac{1}{2} - \frac{\langle w \rangle}{4\langle \tilde{n}_c \rangle} (1 + k^{-1}) - \frac{1}{4\langle \tilde{n}_c \rangle} \right], \quad (13)$$

$$A_f = \langle w \rangle \langle \tilde{n}_c \rangle. \quad (14)$$

Below we shall neglect the last term in expression (13) which is important only for events with a very small  $Q^2$  when  $\langle \tilde{n}_c \rangle < 1$ .

The following qualitative predictions can be obtained from (12):

1) For small  $Q^2$ , the multiplicity distribution of the QCD induced events has large  $k$ , so that it is close to a Poisson distribution. Therefore, for similar values of  $\langle \tilde{n}_c \rangle$  and  $\langle w \rangle$ , the value of  $\rho$  is negative (anticorrelations). Indeed the correlations are negative if

$$\frac{\langle w \rangle}{\langle \tilde{n}_c \rangle} < 2 + 4 \frac{R_f}{R_b}. \quad (15)$$

This relation is expected to be a rather good estimate; From  $e^+e^-$  results one expects that the QCD induced events well increase the particle multiplicity, however, the average first-order QCD multiplicity  $\langle w \rangle$  cannot be much larger than the overall average multiplicity  $\langle \tilde{n}_c \rangle$  of all events (including the first-order QCD).

2) The values of  $k$  decreases with increasing  $Q^2$ . This means that  $\rho$  increases with energy and even can change sign. The increase with  $Q^2$  is mainly determined by the evolution of the average multiplicities  $\langle w \rangle$  and  $\langle \tilde{n}_c \rangle$  as a function of  $Q^2$ .

3) Let us consider the most interesting case when  $Q^2$  is small and fixed. Since, for the current region of the Breit frame, the evolution of the multiplicity distribution is determined only by  $Q^2$  [13],  $A_b$  and  $A_f$  in (12) do not depend on  $x$ . Therefore, (12) has an  $x$ -dependence determined by the production rates  $R_b$  and  $R_f$ .

Since the only dominant process at small  $Q^2$  is the BGF,  $\rho$  in (12) is determined mainly by the behavior of the BGF production rate which increases with decreasing  $x$  due to increase of the gluon density inside the proton. Therefore, one can expect the magnitude of  $\rho$  increases with decreasing  $x$ .

As we see, one of the most striking features of the Breit frame is a negative value of the long-range correlations. Such a prediction is rather unusual for the forward-backward correlations studied so far. For the deep-inelastic processes in the Breit frame, this property is quite clear intuitively: if one or two jets move to the target region, then the fewer particles are observed in the current region, the more particles can be found in the target region and vice versa.

Below we shall see that the analytical observations discussed above are in good agreement with a Monte Carlo simulation.

## 4 Monte Carlo study

We now illustrate the points discussed above using the LEPTO 6.5 Monte Carlo model [14]. The model has been tuned as described in [15]. The hard process in LEPTO is described by a leading order matrix element. Below the matrix-element cut-off, parton emission is based on the parton shower described by the Dokshitzer-Gribov-Lipatov-Altarelli-Parisi evolution equation. The JETSET Monte Carlo [16] based on the LUND String Fragmentation Model is used to describe hadronization. Although the production rate of (2+1) jets seems to be underestimated in LEPTO [17], this Monte Carlo model should be more adequate for illustrating the points discussed above since it is based on an exact first-order QCD matrix element calculation.

To generate deep-inelastic events, the following cuts are used:

$$Q^2 > 10 \text{ GeV}, \quad y \leq 0.95, \quad E \geq 10 \text{ GeV},$$

where  $y$  is the relative energy transferred from the electron to the proton in the proton rest frame,  $E$  is the energy of scattered electron. In total, 200k events are generated for each of the measurements to be discussed below.

## 4.1 First-Order QCD Rates

Let us first analyse the first-order QCD rate for the BGF and QCDC. We define the production rates  $R_{\text{BGF}}$  and  $R_{\text{QCDC}}$  for the BGF and QCDC, respectively, as

$$R_{\text{BGF}} = \frac{N_{\text{BGF}}}{N_{\text{ev}}}, \quad R_{\text{QCDC}} = \frac{N_{\text{QCDC}}}{N_{\text{ev}}}, \quad (16)$$

where  $N_{\text{BGF}}$  and  $N_{\text{QCDC}}$  are the numbers of the BGF and QCDC events. Experimentally, the information about sum of these rates can be obtained from the study of (2+1) jet rate  $R_{2+1}$  [18, 19]. Note that  $R_{\text{BGF}} + R_{\text{QCDC}}$  is not equivalent to  $R_{2+1}$ . The latter depends on the jet algorithm and a resolution scale  $y_{\text{cut}}$  to define jets. Note that the normalizations in  $R_{2+1}$  and (16) can also be different.

For the Monte Carlo study, (16) can directly be obtained by counting the first-order QCD events<sup>1</sup>. The production rates in LEPTO are derived numerically as the integral of the relevant first-order matrix elements.

Fig. 4 shows the production rates of the BGF and QCDC as a function of the  $Q^2$  and the Bjorken variable  $x$ . For the latter, the cut  $Q^2 \leq 50 \text{ GeV}^2$  is used to constrain the effect of increase of  $Q^2$  with increasing  $x$ .

For the  $Q^2$  variable, the BGF rate rises with increasing  $Q^2$  for  $Q^2 < 100 \text{ GeV}^2$ , and then it falls. For  $x$  variable, the BGF rate increases with decreasing  $x$ . Since for all range of  $x$  studied, the average value of  $Q^2$  only increases from  $\sim 19 \text{ GeV}^2$  (for  $\langle x \rangle \sim 0.0007$ ) to  $21 \text{ GeV}^2$  (for  $\langle x \rangle \sim 0.02$ ), such a behavior is mainly because of the variations of  $x$  due to an increase of the gluon density inside proton.

## 4.2 Current-Target Multiplicity Correlations

Fig. 5 shows the behavior of the covariance  $\rho$  as a function of the  $Q^2$  and the Bjorken variable  $x$ . The values of  $\rho$  for the QPM are near zero, i.e. there is no strong linear interdependence between the current and the target regions<sup>2</sup>. This illustrates the fact that the LUND String Fragmentation Model used by LEPTO does not produce large correlations during the formation and an independent breaking of strings stretched between the current-region showering partons and the remnant.

Adding BGF and QCDC events leads to the negative correlations expected. The magnitude of  $\rho$  rises with increasing  $Q^2$  (for  $Q^2 < 100 \text{ GeV}^2$ ) and then falls. Such a behavior is due to the similar trend of the BGF rate shown in Fig. 4. Note that a decrease of  $k$  in (12) can also contribute to the decrease of the correlation. For  $Q^2 < 100 \text{ GeV}^2$ , symbols for QPM+BGF and the LEPTO default (QCD) are very close to each other.

---

<sup>1</sup> The parameter LST(24) specifies the type of the first-order QCD event in LEPTO model.

<sup>2</sup> Note again that, generally, a non-linear interdependence may exist.

The dependence of  $\rho$  as a function of  $x$  is mainly due to the variation of  $x$ , since there are no large variations in  $Q^2$  for the cuts applied. The magnitude of  $\rho$  increases with decreasing  $x$ . Symbols for the QPM with all first-order QCD effects (QPM+BGF+QCDC) and for QPM+BGF events are on top of each other, i.e. the boson-gluon fusion is the main source of the correlation. For larger  $x$ , symbols become distinguishable since the contribution of the BGF becomes smaller at large  $x$ .

According to the analytical expression (12), there exists the linear relationship between the  $\rho$  and the probabilities  $R_b$  and  $R_f$  determining the BGF production rate. The solid line shown in Fig. 5 illustrates the BGF rate (see Fig. 4) multiplied by the scale factor  $-6.5$ . The shaded band shows statistical errors for the BGF rate. As seen, the behavior of  $\rho$  follows that of the BGF rate rather well.

Note that for very small  $x$ , one has to expect a deviation from the linear relationship between  $\rho$  and the BGF rate since the non-linear term omitted in (10) cannot be longer neglected.

## 5 Conclusion

Long-range correlations in ep collisions were investigated using the Breit frame. It was shown that the correlations between the current and the target regions of the Breit frame are sensitive to the first-order QCD processes leading to the (2+1) jets. In particular, at small  $x$  and a restricted interval of  $Q^2$ , the strength of the long-range correlations is mainly determined by the boson-gluon fusion processes. One of the distinguishing properties of the correlations is a negative value and rise in the magnitude with decreasing  $x$ .

This method can be used to study the production rates of the boson-gluon fusion processes, to understand better the gluon density inside proton and to discriminate between different Monte Carlo models used to simulate the deep-inelastic processes. The approach has the advantage that it is simple and does not involve any jet algorithm and a resolution scale necessary to determine jet, since it is based on purely topological properties of (2+1) jets in the Breit frame. Therefore, the advantage of this method is absence of the systematical uncertainties connected with the ambiguity in determining jets.

Note also that the jet definitions are not able to distinguish between the proton remnant and QCD induced jets if they are close to each other. This problem is avoided in the proposed jet-rate measurement: The strength of the correlations is determined on the basis of an enhancement of the multiplicity in the target region for the first-order QCD events, rather than resolving well-separated jets.

The current-target correlations can be used to study a difference in particle spectra between the current region of deep-inelastic scattering events and a single

hemisphere of  $e^+e^-$  interactions. In contrast to deep-inelastic scattering processes exhibiting anticorrelations in the Breit frame, the forward-backward correlations between two opposite rapidity hemispheres of  $e^+e^-$  annihilations are positive [3–5]. This may lead to discrepancies in attempts to compare the current region of ep collisions in the Breit frame with a single hemisphere of  $e^+e^-$  interactions.

Estimating the current-target multiplicity correlations analytically, we did not take into account possible color exchange effects between the fragmentation of the outgoing partons and that of the remnant. Also we did not discuss high-order QCD corrections. These topics are rather important for a quantitative confrontation of the correlations with the data and have to be studied in future.

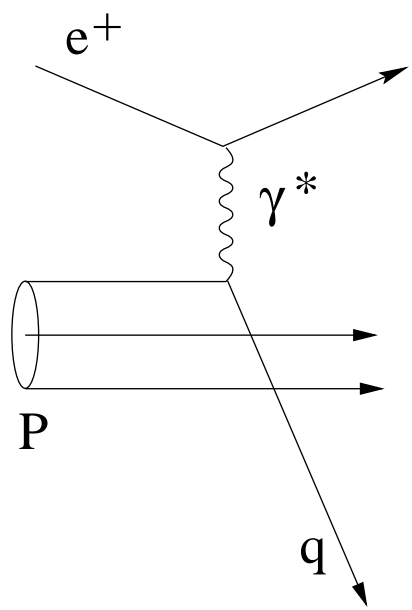
## 6 Acknowledgments

I thank M.Derrick, T.Doyle, L.Lönnblad, S. Magill, J.Repond, L.M.Shcheglova and A.N.Solomin for valuable discussions.

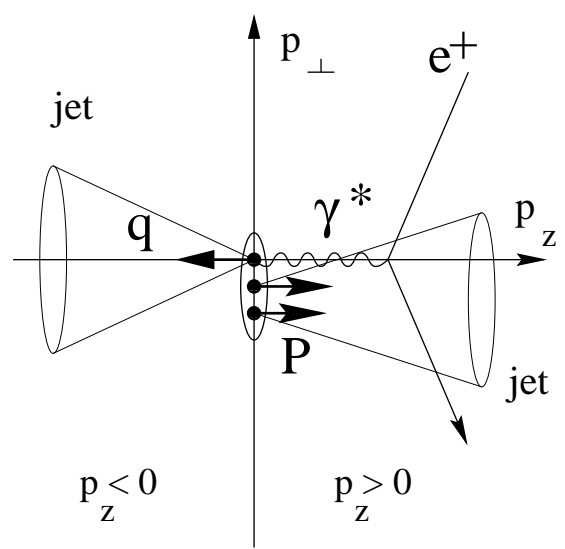
## References

- [1] M.Althoff et al., Z.Phys. C **29**, 347 (1985);  
M.Derrick et al., Phys. Rev. D **34**, 3304 (1986); Z.Phys. C **35**, 323 (1987);  
TASSO Coll., W.Braunschweig et al., Z.Phys. C **45**, 193 (1987)
- [2] M.Arneode et.al. Nucl. Phys. B **258**, 249 (1985)
- [3] DELPHI Coll., P.Abreu et al., Z.Phys. C **50**, 185 (1991)
- [4] Y.G.Xie (for the ALEPH Coll.,) XXI Int. Symp. on Multiparticle Dynamics, Wuhan, China, 1991, Ed. W.Yuanfong, L.Lianshou, (World Scientific, Singapore, 1992) p.172
- [5] OPAL Coll., R. Akers et al. Phys. Lett. B **320**, 417 (1994);  
M.Cuffiani (for the OPAL Coll.,) XXIX Int. Symp. on Multiparticle Dynamics, Vietri sul Mare, Selerno, Italy, 1994, Ed. A.Giovannini et al., (World Scientific, Singapore, 1995) p.37
- [6] H.Grässler et al., Nucl. Phys. B **223**, 267 (1983)
- [7] T.Kafka et al., Phys. Rev. Lett. **34**, 687 (1975);  
S.Uhlig et al., Nucl. Phys. B **132**, 15 (1978);  
K.Alpgard et al., Phys. Lett. B **123**, 601 (1983);  
G.J.Alner et al., Nucl. Phys. B **291**, 445 (1987);  
R.E.Ansgore et al., Z.Phys. C **37**, 191 (1988)
- [8] NA22 Coll., V.V.Aivazyan et al., Z.Phys. C **42**, 533 (1989)
- [9] P. Van Mechelen, Proc. of 5th Int. Workshop “Deep Inelastic Scattering and QCD” Chicago, 1997, Ed. J. Repond and D.Krakauer (AIP, New York, 1997) p.602
- [10] R.P.Feynman, Photon-Hadron Interactions, Benjamin, NY, 1972
- [11] A.Wróblewski, XV Int. Symp. on Multiparticle Dynamics, LUND, Sweden 1984, Ed. G.Gustafson and C.Peterson, (World Scientific, Singapore, 1984) p.30
- [12] K.H.Streng, T.F.Walsh, P.M.Zerwas, Z.Phys. C **2**, 237 (1979)
- [13] L.V.Gribov, Yu. L. Dokshitzer, S.I.Troyan, V.I.Khoze, Zh. Eksp. Teor. Fiz. **94**, 1303 (1988)
- [14] G.Ingelman, A.Edin, J.Rathsman, DESY 96-057

- [15] N.Brook et al., Proc. of the Workshop 1995/1996 “Future Physics at HERA”, Ed. G. Ingelman et al., (DESY, 1996), p.613
- [16] T.Sjöstrand, Computer Phys. Commun. **82**, 74 (1994)
- [17] See, for example, M.Wobish (H1 Coll.) Proc. of 5th Int. Workshop “Deep Inelastic Scattering and QCD” Chicago, 1997, Ed. J. Repond and D.Krakauer (AIP, New York, 1997) p.699
- [18] H1 Coll., I.Abt et al., Z.Phys. C **61**, 59 (1994)
- [19] ZEUS Coll., M.Derrick et al. Z.Phys. C **67**, 81 (1995)



**a)**



**b)**

Figure 1: a) Diagram for the neutral current deep-inelastic scattering in the QPM; b) A schematic representation of the Breit frame. Particles with  $p_z < 0$  belong to the current region. Particles with  $p_z > 0$  form the target region.

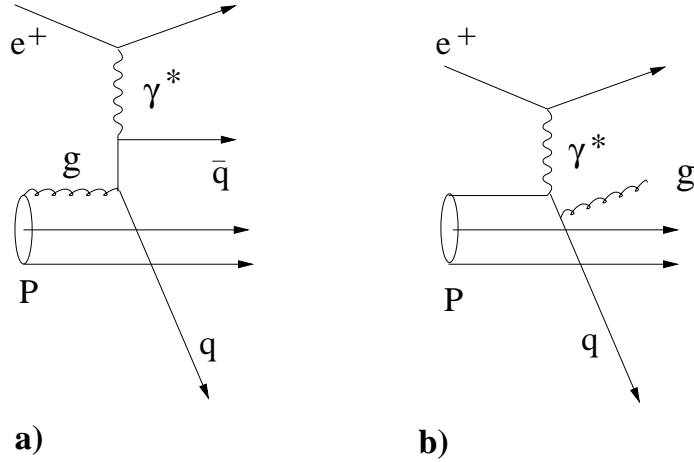


Figure 2: *Diagrams in the first-order perturbative QCD: 1) Boson-Gluon Fusion (BGF); 2) QCD Compton scattering (QCDC). For the latter diagram the gluon can also be radiated before the interaction with  $\gamma^*$ .*

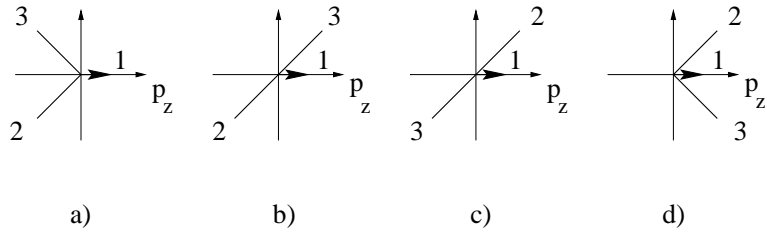


Figure 3: *Typical configurations of (2+1) jets in the Breit frame [12]. "1" denotes the proton remnant, "2" and "3" are jets due to the first-order QCD corrections to the parton model. Jets with  $p_z < 0$  form the current region. For  $p_z > 0$ , they belong to the target region.*

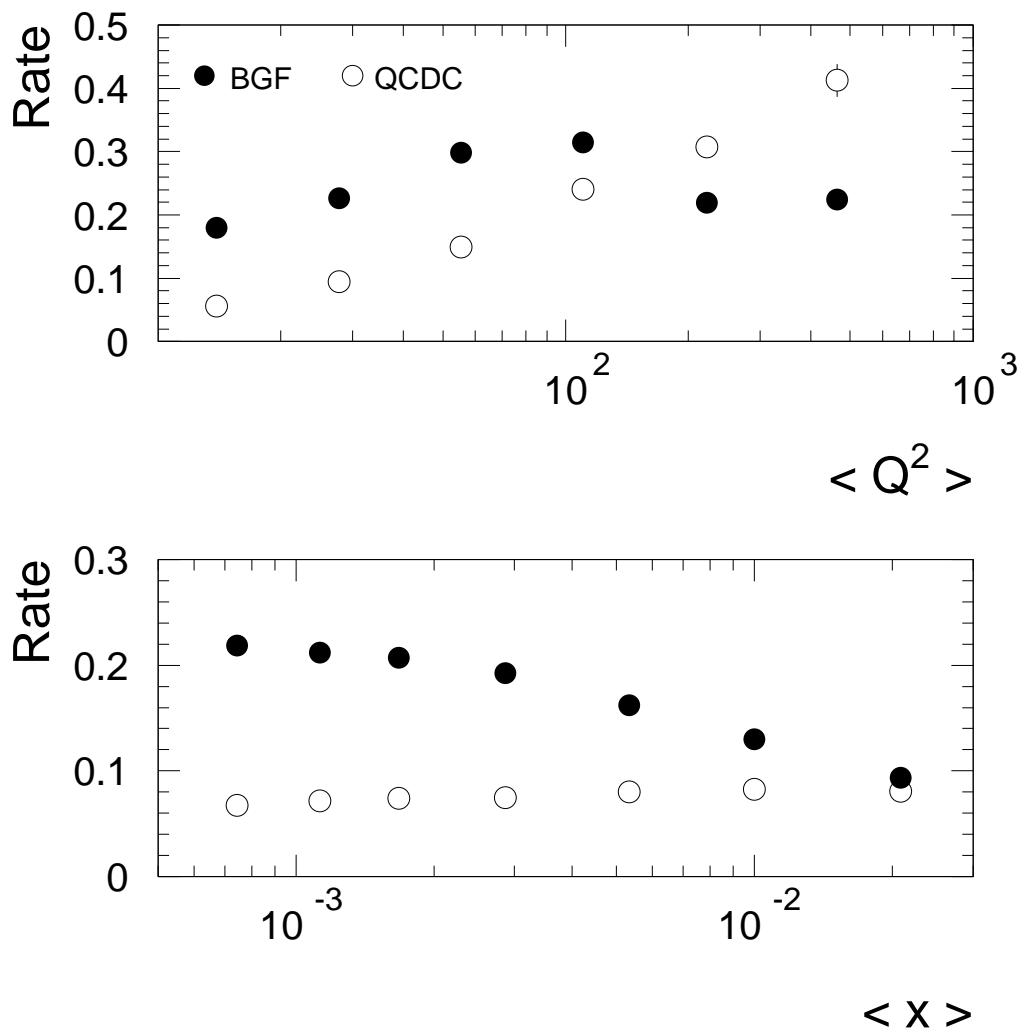


Figure 4: Production rates for the BGF and QCDC as a function of  $Q^2$  and  $x$ .

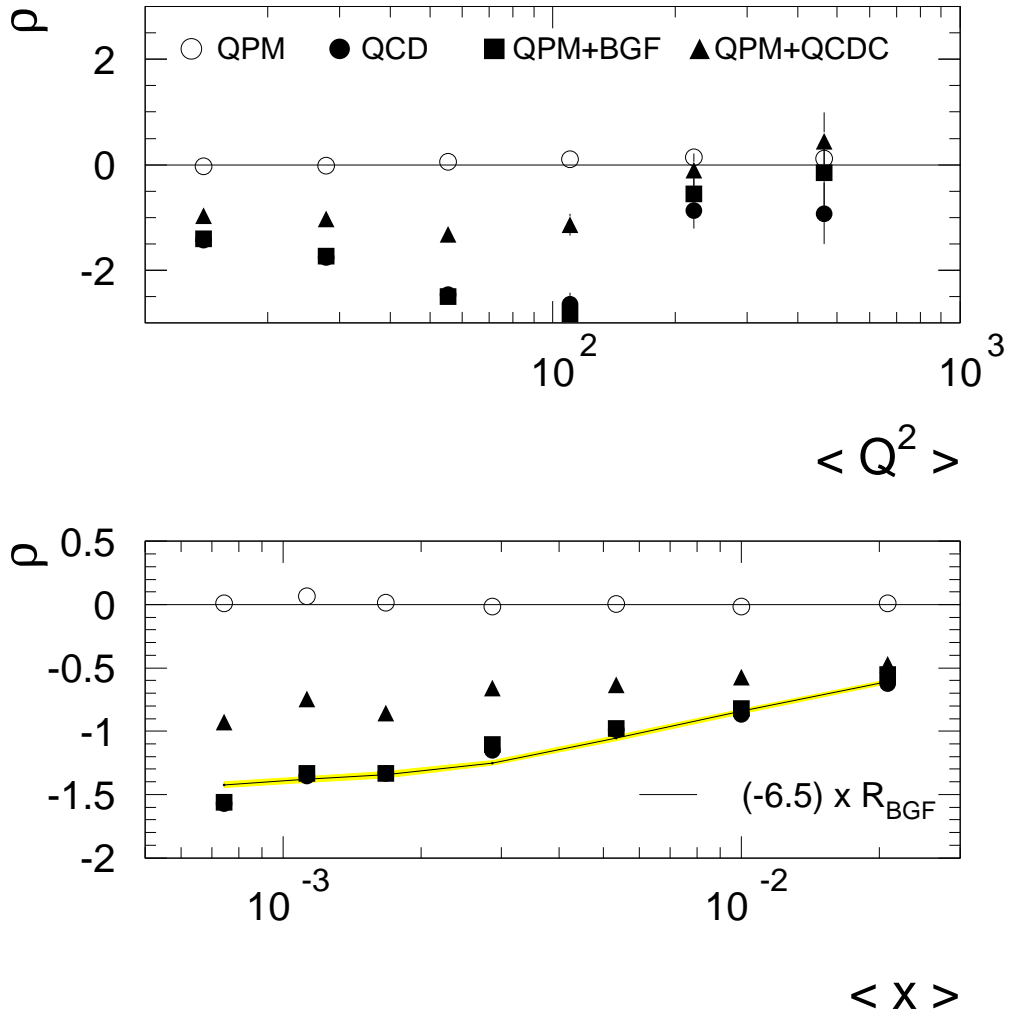


Figure 5: The values of the covariance  $\rho$  for different bins in  $\langle Q^2 \rangle$  and  $\langle x \rangle$  obtained from the LEPTO 6.5 Monte Carlo model. We show four event topologies: 1) quark-parton model (QPM); 2) QPM with the first-order QCD events (QPM+BGF+QCDC) 3) QPM with BGF events; 4) QPM with QCDC events. For the latter figure, symbols for QPM+BGF+QCDC and QPM+BGF are on top of each other.